Strain Capacity of High-Strength Line Pipes†

SUZUKI Nobuhisa[*1] KONDO Joe[*2] SHIMAMURA Junji[*3]

Abstract:

Two compression and two bending tests using X80 high-strain line pipes with 30 inches (762 mm) in outside diameter were conducted to investigate its compression capacity and bending capacity. The compression test revealed that the pipes had the critical compressive strain of 0.90 and 0.78% and the bending test clarified that the 2OD (two times outside diameter) average critical compressive strains were 2.40 and 2.15% and the 1OD average were 2.67 and 2.28%, respectively. The test results proved that X80 high-strain linepipes satisfy requirements from pipeline projects and ensure pipeline integrity in seismic and permafrost areas.

1. Introduction

The operators of long-distance ultrahigh-pressure gas pipeline projects overseas are now examining the prospects for cost reduction by the application of high-strength line pipes[1]. When pipelines are constructed in seismic areas and permafrost areas, high-strength line pipes are required to provide a sufficient strain capacity. High-strength line pipes are generally recognized to have a reduced strain capacity compared to lower strength line pipes. High-strain line pipes (high-strain LPs—HSLPs), on the other hand, have a strain capacity sufficient to withstand compression and bending deformation in spite their high strength[2–4].

In this paper, the authors describe a series of compression and bending tests conducted to investigate the strain capacity of HSLPs. The tests were performed using API 5L Grade X80 pipe with an outside diameter of 762 mm and wall thickness of 15.6 mm. Four pipes were tested in total, two by the compression test and two by the bending test. In this paper, the authors describe the results of these tests on actual pipes and compare them with analytical solutions related to compression buckling. The authors also compare the test results with the results of FEA (finite element analysis) and clarify how the geometric imperfections of pipes affect the strain capacity.

2. Outline of the Compression Test and Bending Test

2.1 Apparatus and Test Pipes for the Compression Test

The compression test was performed with a 140-MN press (the test apparatus is shown in **Photo 1**). The two test pipes, C-1 and C2, were tested without internal pressure. Each test pipe had a total length of 1 840 mm,

Photo 1 Compression test apparatus

† Originally published in *JFE GIHO* No. 17 (Aug. 2007), p. 31–36

[*1] Dr. Eng., P.E.
Principal Researcher,
JFE R&D

[*2] Manager, Shape Sec.,
Products Design & Quality Control for Steel Products Dept.,
West Japan Works,
JFE Steel

[*3] Senior Researcher Staff Assistant Manager,
Plate & Shapes Res. Dept.,
Steel Res. Lab.,
JFE Steel

Table 1 Dimensions and tensile properties of test pipes

Pipe No.	Dimensions			Longitudinal tensile properties			
	OD (mm)	WT (mm)	OD/WT	YS (MPa)	TS (MPa)	Y/T (%)	uEL (%)
C-1	762	15.6	49	524	684	77	8
C-2				565	704	80	8

OD: Outside diameter WT: Wall thickness YS: Yield strength
TS: Tensile strength YS/TS: Yield ratio uEL: Uniform elongation

outside diameter (OD) of 762 mm, wall thickness (WT) of 15.6 mm, and thickness-diameter ratio (OD/WT) of 49. **Table 1** shows these pipe dimensions, as well as the tensile properties of the pipes in the axial direction.

2.2 Apparatus and Test Pipes for the Bending Test

The apparatus for the bending test was composed of a test pipe, a sleeve pipe, a moment arm, a hydraulic jack, and a main frame (**Photo 2**). Each test pipe (B-1 and B2) had an outside diameter of 762 mm, a wall thickness of 15.6 mm, and a pipe length of 4 000 mm. The moment arm had a length of 1 830 mm and span of 5 810 mm. Though an internal pressure of 12 MPa was applied, the test pipe was subjected to axial tension and bending deformation since the internal pressure also acted on both of the end caps. **Table 2** shows the dimensions of the test pipes and their mechanical properties in the axial direction. The outside diameter and wall thickness of the pipes used for the bending test (B-1 and B-2) were identical to those of the pipes used for the compression test (C-1 and C-2).

Photo 2 Bending test apparatus

Table 2 Dimensions and tensile properties of test pipes

Pipe number	Dimensions			Longitudinal tensile properties			
	OD (mm)	WT (mm)	OD/WT	YS (MPa)	TS (MPa)	Y/T (%)	uEL (%)
B-1	762	15.6	49	535	696	77	8
B-2				672	782	86	8

OD: Outside diameter WT: Wall thickness YS: Yield strength
TS: Tensile strength YS/TS: Yield ratio uEL: Uniform elongation

Table 3 Geometric imperfections of the test pipes

Geometric imperfections			Test pipe	
			C-1, B-1	C-2, B-2
OD (Outside diameter) (mm)		Min.	761.6	760.0
		Max.	763.0	761.9
WT (Wall thickness) (mm)		Min.	15.52	15.59
		Max.	15.90	15.66
BL (Longitudinal blister)	Wave length (mm)		740–800	740–800
	Amplitude (mm)		0.5	0.5

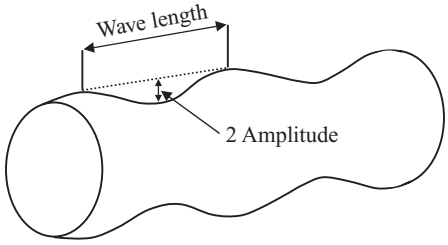

Fig. 1 Definition of longitudinal blister

2.3 Geometric Imperfections

The geometric imperfections of the test pipes are shown in **Table 3**. The geometric imperfections were measured using lattice lines and lattice points drawn on the test pipe surfaces (Photos 1 and 2). The geometric imperfections were imperfections of the outside diameter, wall thickness, and longitudinal blister of the pipes. The definitions of the longitudinal blister are shown in **Fig. 1**. These geometric imperfections are expressed as an OD imperfection, a WT imperfection, and a BL imperfection in the following figures, respectively.

3. Strain Capacity of High-Strain Line Pipes to Withstand Compression

3.1 Results of the Compression Test

The results of the compression test on pipes C-1 and C-2 are shown in **Figs. 2** and **3**. As shown in Fig. 2, the critical compressive stress of test pipe C-1 was 568 MPa and the critical compressive strain of C-1 was 0.90%. As shown in Fig. 3, the critical compressive stress of C-2 was 579 MPa and the critical compressive strain of C-2 was 0.78%. The critical compressive strain of C-1, meanwhile, was larger than that of C-2 because of the lower yield ratio of the former. Test pipe C-2 had a higher yield stress than C-1, hence it had a larger critical compressive stress.

3.2 Comparison of Test Results with the Analytical Solution

The stress-strain relationship of materials is

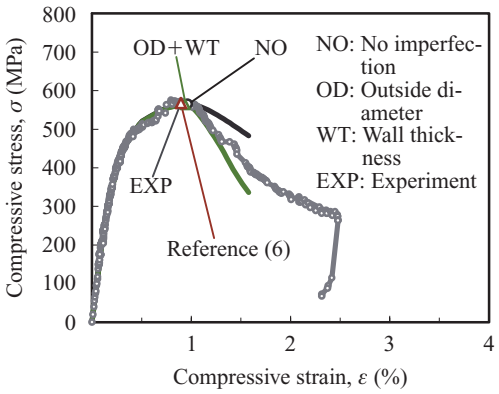

Fig. 2 Compressive deformation of Pipe C-1

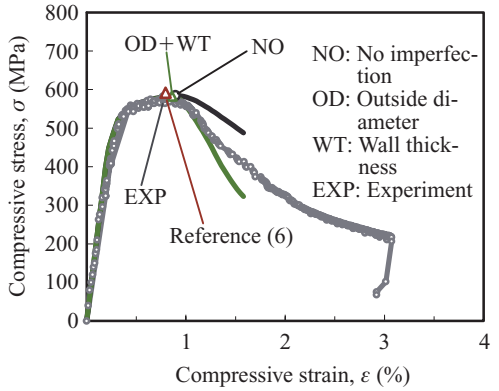

Fig. 3 Compressive deformation of Pipe C-2

expressed by the Ramberg-Osgood formula[5] (the R-O formula). An analytical solution[6] related to the compressive critical strain of a thin-walled cylindrical shell is given in the following equations:

$$\left(\frac{\sigma_{cr}}{\sigma_0}\right)^N = -\frac{1}{2\alpha}\left(1+\frac{1}{N}\right)+\frac{4}{3\alpha\sqrt{N}}\frac{E}{\sigma_0}\frac{t}{D} \cdots (1)$$

$$\varepsilon_{cr} = \frac{\sigma_0}{E}\left(\frac{\sigma_{cr}}{\sigma_0}\right)+\frac{\alpha\sigma_0}{E}\left(\frac{\sigma_{cr}}{\sigma_0}\right)^N \cdots (2)$$

where E is Young's modulus, σ and σ_0 are R-O parameters, ε_{cr} is critical compressive stress, and ε_{cr} is critical compressive strain.

The R-O parameters and material constants of test pipes C-1 and C-2 are shown in **Table 4**. When these are substituted in the above-described analytical solution, the critical compressive stress and critical compressive strain of test pipe C-1 become 569 MPa and 0.93%, respectively. For test pipe C-2, these values become 592 MPa and 0.80%, respectively. As shown in Figs. 2 and 3, the calculation results agree well with the test data.

Table 4 Ramberg-Osgood parameters for the test pipes

Pipe number	R-O parameters				
	E (GPa)	ε_0 (%)	σ_0 (MPa)	α	N
C-1	206	0.5	524	0.965	11.82
C-2	210	0.5	565	0.858	17.28

E: Young's modulus ε_0: 0.5% strain σ_0: Stress at ε_0
α, N: R-O parameters

3.3 Comparison of the Test Results with the Results of the Finite Element Analysis

The compressive deformation behavior of test pipes C-1 and C-2 was analyzed without considering the geometric imperfections. The test pipes were modeled by four-node shell elements. Mesh dimensions of 40 nm in the circumferential direction and 25 mm in the longitudinal direction were adopted. The FEA results related to C-1 and C-2 are shown in Figs. 2 and 3, respectively.

As shown in Figs. 2 and 3, the results of the FEA and the test results agree well with each other in the range up to the peak load. According to the FEA in which the geometric imperfections were neglected, the critical compressive stress and critical compressive strain of test pipe C-1 were 562 MPa and 0.88%, respectively, while those for C-2 were 581 MPa and 0.80%, respectively. Given that these calculation results were all close to the test results, we speculate that it may be possible to estimate the critical compressive stress and critical compressive strain of the test pipes with good accuracy by FEA even neglecting the geometric imperfections.

Figures 2 and 3 also show the FEA results in which the (OD + WT) imperfections were considered for test pipes C-1 and C-2. As shown in the figures, the calculation results in which the (OD + WT) imperfections were considered agree well with the test results in the range up to the critical compressive stress. The critical compressive stress and critical compressive strain of test piece C-1 were 561 MPa and 0.87%, respectively, while those for C-2 were 580 MPa and 0.80%, respectively. After the reaching of the maximum compressive stress, the calculation results in which the (OD + WT) imperfections were considered decreased earlier than the results in which the geometric imperfections were considered.

To sum up the above-described results, the geometric imperfections have little effect on the critical compressive stress and critical compressive strain of pipes subjected to compressive deformation. That is, during the growth of a shell wrinkle of a pipe subjected to compressive deformation, the effect of a boundary condition that constrains the radial displacement is remarkable at the pipe ends, while the effect of the geometric imperfections does not manifest itself clearly.

3.4 Comparison of Shell Wrinkles

Photo 3 shows the post-buckling behavior of test pipe C-1. A shell wrinkle occurred at the end of the

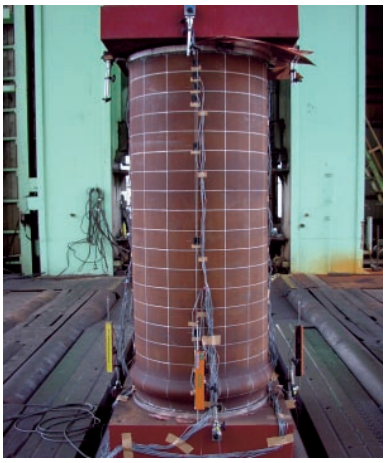

Photo 3 Shell wrinkle after a compression test

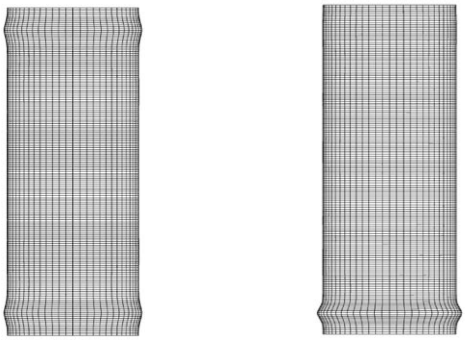

Fig. 4 Effect of geometric imperfections on shell wrinkling

pipe near the bottom. The same deformation state was observed in test pipe C-2.

The shell wrinkle of test pipe C-1 obtained in the FEA is shown in **Fig. 4**. The left-hand and right-hand figures show the results of the calculations that neglect the geometric imperfections (OD + WT) and that consider the imperfections, respectively. The average compressive axial strain was 2.1% in both cases. The shell wrinkle appeared at both the top and bottom ends of the test pipe when the geometric imperfections were neglected, whereas it appeared only at the bottom end of the test pipe when the geometric imperfections were considered. The shell wrinkle that appeared when the geometric imperfections were considered closely resembled the shell wrinkle shown in Photo 3.

4. Strain Capacity of High-Strain Line Pipes to Withstand Bending

4.1 Results of the Bending Test

Figures 5 and **6** show the relationship between the bending moment and average bending strain of test pipe B-1, while **Figs. 7** and **8** show this relationship in B-2. In each figure, the average bending strain of the abscissa

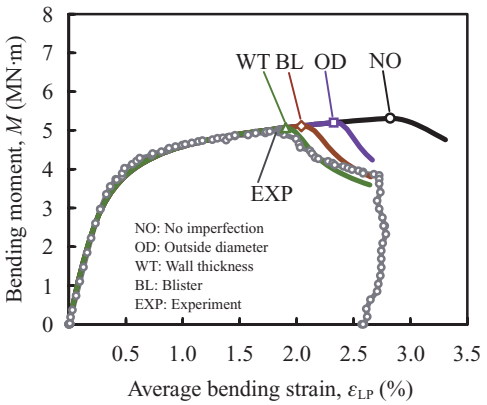

Fig. 5 Moment vs. average bending strain of Pipe B-1

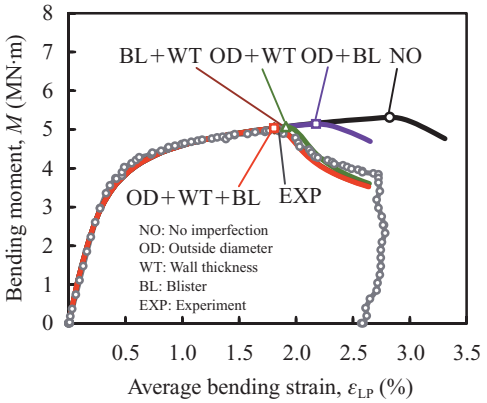

Fig. 6 Moment vs. average bending strain of Pipe B-1

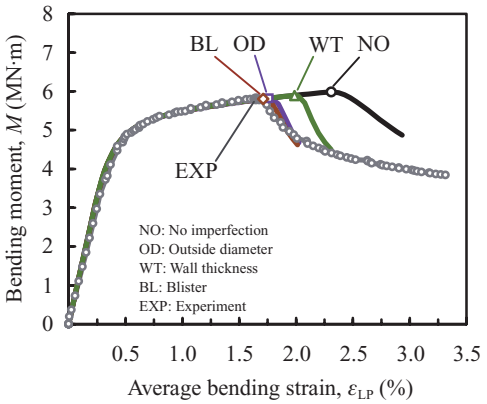

Fig. 7 Moment vs. average bending strain of Pipe B-2

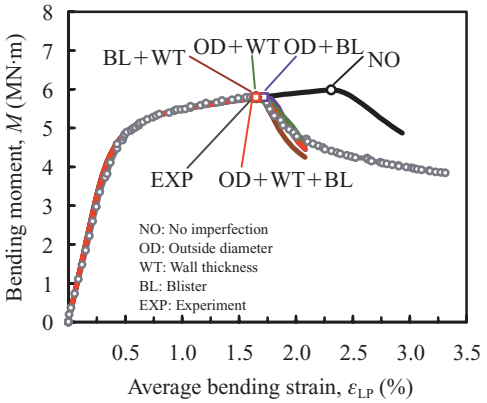

Fig. 8 Moment vs. average bending strain of Pipe B-2

is a value found from the relative rotation angle of the total length of the test pipe and indicates an average bending strain relative to the total pipe length.

As shown in the figures, the critical bending moment and average bending strain of test pipe B-1 were 5.08 MN·m and 1.85%, respectively, while those of B-2 were 5.80 MN·m and 1.65%. The critical bending moment of B-1 was 22% smaller than that of B-2, and the average bending strain of B-1 was 20% larger than that of B-2.

4.2 Finite Element Analyses of the Bending Tests

Test pipes B-1 and B-2 were modeled using four-node shell elements by the same method applied in the FEA for the compression test pipes (C-1 and C-2). The divided elements for B-1 and B-2 were the same as those for C-1 and C-2. The sleeve pipe of the test apparatus was modeled by four-node shell elements and the moment arm was modeled by beam elements.

4.2.1 Finite element analysis of test pipe B-1

Figure 5 shows the results of FEA in which a single geometric imperfection was considered for test pipe B-1. The abscissa in the figure indicates the bending moment and the ordinate indicates average bending strain. The figure also plots the test results for test pipe B-1 for comparison. As shown in the figure, both the critical bending moment and average critical bending moment reach their maximums in the calculations that neglect the geometric imperfections.

The results of the FEA in which the geometric imperfections were neglected agree well with the test data in the range up to the critical deformation. However, the deformation increases even after the critical deformation, and eventually the critical average strain is over estimated. The results of the other calculation which considered a single geometric imperfection apparently showed the same tendency. However, the estimation accuracy of the critical average increases in the following order: OD imperfection, BL imperfection, WT imperfection.

Figure 6 shows the results of the calculation that considers multiple geometric imperfections in combination for test pipe B-1. The abscissa and ordinate of the figure are the same as those in Fig. 5, and the test results for B-1 are also plotted for comparison. A comparison of the results reveals that the values obtained when the (OD + WT) imperfections were considered were larger than the test data. The calculation that considered the (BL + WT) imperfections and the calculation that considered the (OD + WT + BL) imperfections produced the same result. The calculation results were conservative compared to the experimental results.

4.2.2 Finite element analysis of test pipe B-2

Figure 7 shows calculation results in which a single geometric imperfection was considered for test pipe B-2. The abscissa and ordinate of the figure are the same as those in Fig. 5, and the test results for test pipe B-2 are also plotted for comparison. The results of the calculation that neglects the geometric imperfections show the same tendency as in Fig. 5 and agree well with the results of the other calculations. The estimation accuracy of the critical average bending strain in which a single geometric imperfection was considered increases in the following order: WT imperfection, OD imperfection, BL imperfection.

The difference between the B-2 and B-1 calculation results is reflected in the results of a calculation that considers a WT imperfection. Because the WT imperfection of B-2 is smaller than the WT imperfection of B-1, the critical average strain obtained when the WT imperfection was considered was close to the result obtained when the geometric imperfections were neglected, and was larger than the value calculated for B-1.

Figure 8 shows the relationship between the bending moment and average bending strain in calculations that consider multiple geometric imperfections. The average critical bending strain calculated when an (OD + WT) moment was considered was slightly larger than the value obtained in the test. The average critical bending strain obtained when a (BL + WT) imperfection or an (OD + WT + BL) imperfection was considered was equal to the test data, and values close to the experimental data were obtained. As described above, the small WT imperfection in test pipe B-2 led to large errors in the calculation in which the WT imperfection was considered for B-2, relative to the experimental results. However, as shown in the figure, the results obtained from the calculation that considered a WT imperfection and other geometric imperfections in combination were close to the experimental results.

4.3 Comparison of Shell Wrinkles

Photo 4 shows the growth state of a shell wrinkle of test pipe B-1. The shell wrinkle was generated on the outer surface of the crest of the test pipe, 125 mm to the left of the pipe center.

Figure 9 shows a shell wrinkle that appeared on test pipe B-1 when geometric imperfections were neglected, and **Fig. 10** shows a shell wrinkle that appeared on B-1 when the (OD + WT) imperfections were considered. Two shell wrinkles appeared when geometric imperfections were neglected, whereas one shell wrinkle appeared when the (OD + WT) imperfections were considered. The shell wrinkle in the latter case had almost the same shape and appeared at almost the same position

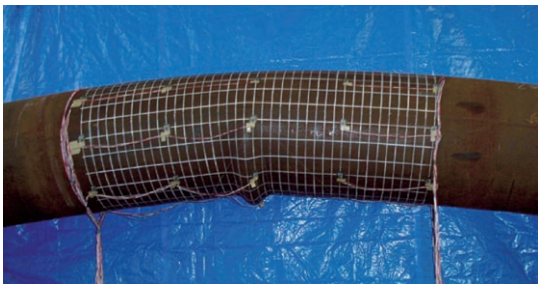

Photo 4 Shell wrinkle of Pipe B-1

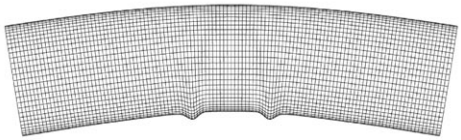

Fig. 9 Shell wrinkles with no geometric imperfection

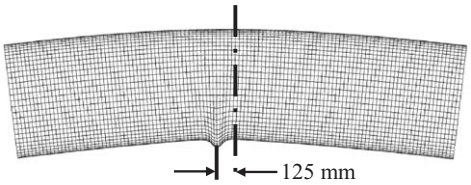

Fig. 10 Shell wrinkle with the OD+WT imperfections

as the shell wrinkle observed in the bending test shown in Photo 4.

4.4 Average Critical Compressive Strain

In Section 4.2 above, the strain capacity of an X80-HSLP LP based on the bending test is expressed as the average critical bending strain. In this section, however, we express the strain capacity using the average critical strain, an average of the compressive strain. **Figure 11** shows the relationship among bending strain, compressive strain, and tensile strain in a section of test pipe B-1 very close to a shell wrinkle.

The average critical compressive strain generated when the gauge length is defined as the total length (L_p) is expressed as ε_{crLp}. The average critical compressive strains generated when the gauge length is the pipe outside diameter (1D) and twice (2D) are expressed as ε_{crD} and ε_{cr2D}, respectively.

The values of the average critical compressive strain (ε_{crLp}, ε_{cr2D}, ε_{crD}) obtained in the bending test for test pipe B-1 were 1.91%, 2.40%, and 2.67%, respectively. In the FEA, the most conservative high-accuracy results were obtained even when the (OD + WT + BL) imperfections were considered, and the values of the critical average compressive strains were 2.01%, 2.28%, and 2.40%. As is apparent from this result, the average critical strain increases as the gauge length decreases.

The values of average critical compressive strain

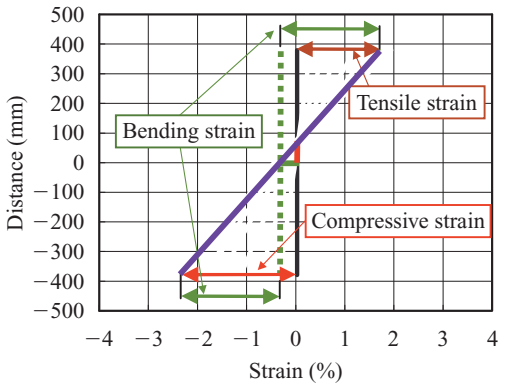

Fig. 11 Longitudinal strain distribution in a pipe section

(ε_{crLp}, ε_{cr2D}, ε_{crD}) obtained in the bending test for test pipe B-2 were 1.85%, 2.15%, and 2.21%, respectively. The values of the average critical compressive strain obtained when the (OD + WT + BL) imperfections were considered were 1.84%, 2.12%, and 2.21%. As with test pipe B-1, the average compressive critical strain increased as the gauge length decreased. Because the YS/TS of test pipe B-2 is larger than that of B-1, the average critical compressive strain of B-2 was smaller than that of B-1.

To sum up the calculation results of the FEA related to test pipes B-1 and B-2, we conclude that we can accurately estimate the strain capacity of pipes to withstand bending by considering multiple geometric imperfections, including a WT imperfection. Three combinations of geometric imperfections can be used to ensure accuracy in this estimation: (OD + WT) imperfections, (WT + BL) imperfections, and (OD + WT + BL) imperfections.

5. Conclusions

To investigate the strain capacity of X80-HSLP, we conducted a compression test and a bending test on test pipes with an outside diameter of 762 mm and a wall thickness of 15.6 mm.

The results of the compression test and FEA conducted on test pipes C-1 and C-2 can be summarized as follows:

(1) The critical compressive strains of test pipes C-1 and C-2 were 0.90% and 0.78%, respectively.
(2) The critical compressive stress and critical compressive strain estimated by the analytical solution and by the FEA agreed well with the test results.
(3) Geometric imperfections did not affect the strain capacity of the pipe to withstand compression, though they did affect shell wrinkling and the post-buckling behavior.

The results of the bending test and FEA conducted on test pipes C-1 and C-2 can be summarized as follows:

(1) The average critical bending strains (20D average) of test pipes B-1 and B-2 were 2.40% and 2.15%,

respectively.

(2) The effect of geometric imperfections on the strain capacity of the test pipes to withstand bending and the post-buckling behavior of the test pipes was remarkable.

(3) The maximum bending moments and average critical strains of pipes can be estimated with good accuracy by considering combinations of geometric imperfections, for example, (OD + WT) imperfections, (BL + WT) imperfections, and (OD + WT + BL) imperfections.

As described above, high-strain line pipes have excellent strain capacity to withstand compression and bending, and are effective in ensuring the integrity of pipelines in seismic areas and permafrost areas.

References

1) Glover, A. Application of Gade 550 (X80) and Grade 690 (X100) in Arctic Climates. Proc. of Pipe Dreamers' Conference on Application and Evaluation of High-Grade Linepipes in Hostile Environments. 2002.
2) Suzuki, N.; Endo, S.; Yoshikawa, M.; Toyoda, M. Effect of Strain-hardening Exponent on Inelastic Local Buckling Strength and Mechanical Properties of Linepipes. Proc. of the 20th OMAE. 2001, paper no. OMAE2001/MAT 3104.
3) Suzuki, N.; Glover, A.; Zhou, J.; Toyoda, M. Bending Capacity of High Strength Line Pipe. Proc. of the 4th Int. Conf. on Pipeline Technology. 2004, vol. 3, p. 1361–1374.
4) Suzuki, N.; Kondo, J.; Endo, S.; Ishikawa, N.; Okatsu, M.; Shimamura, J. Effect of Geometric Imperfection on Bending Capacity of X80 Linepipe. Proc. of the 6th Int. Pipeline Conf. 2006, paper no. IPC2006-10070.
5) Ramberg, W.; Osgood, W. R. Description of Stress-Strain Curves by Three Parameters. NACA. TN. 902, 1943.
6) Suzuki, N.; Toyoda, M. Critical Compressive Strain of Linepipes Related to Work-Hardening Parameters. Proc. of the 21st Int. Conf. on Offshore Mechanics and Engineering. 2002, paper no. OMAE2002 -28253.